NPL
National Physical Laboratory

Report

NPL REPORT
DEPC MPR 056

Review of Techniques for the Characterisation of Residual Stress in Polymer Composites

A S Maxwell, W R Broughton, M J Lodeiro

NOT RESTRICTED

December 2006

dti
National Measurement System

National Physical Laboratory | Hampton Road | Teddington | Middlesex | United Kingdom | TW11 0LW

Switchboard 020 8977 3222 | **NPL Helpline** 020 8943 6880 | **Fax** 020 8943 6458 | **www.npl.co.uk**

dti

The DTI drives our ambition of 'prosperity for all' by working to create the best environment for business success in the UK. We help people and companies become more productive by promoting enterprise, innovation and creativity.

We champion UK business at home and abroad. We invest heavily in world-class science and technology. We protect the rights of working people and consumers. And we stand up for fair and open markets in the UK, Europe and the world.

The National Physical Laboratory is operated on behalf of the DTI by NPL Management Limited, a wholly owned subsidiary of Serco Group plc

Review of Techniques for Characterisation of Residual Stress in Polymer Composites

A S Maxwell, W R Broughton, M J Lodeiro
Engineering and Process Control Division

ABSTRACT

Residual stresses are tensile or compressive stresses that exist in materials without an external load being applied to the component. Their presence in a component can be detrimental to both the performance of a material and the life expectancy of the component. Residual stresses are significantly more difficult to measure than the applied stresses. For this reason, designers and engineers are often forced into using higher safety factors that leads to both overdesign of structures and increased weight. The level of residual stress present in composites is particularly large due to the mismatch in the mechanical properties of the reinforcement and the matrix that forms the composite structure. For this reason it is essential to have techniques that can predict the residual stresses that are present in composite structures. This report reviews the different techniques that can be used to measure residual stresses in composites and the models that have been developed to predict their distribution.

ISSN 1744-0270

National Physical Laboratory
Hampton Road, Teddington, Middlesex, TW11 0LW

We gratefully acknowledge the financial support of the UK Department of Trade and Industry (National Measurement System Policy Unit)

Approved on behalf of the Managing Director, NPL,
by Dr M G Cain, Knowledge Leader, Materials Processing Team,
authorised by Director, Engineering and Process Control Division

CONTENTS

1 INTRODUCTION

Residual stresses are tensile or compressive stresses that exist in materials without an external load being applied to the component. They may appear either during manufacture, assembly or during the service life of the component. These stresses appear in composites materials mainly due to the mismatch in the mechanical properties of the resin and reinforcement. The extent of the residual stresses in a composite will therefore depend largely on the properties of the matrix, fibres and the configuration of the plies.

Residual stresses can be defined as either macroscopic or microscopic in nature [1]. The difference in the thermal coefficients of expansion of the resin and the fibres causes the development of microscopic residual stresses in composites. The high thermal expansion coefficient of the resins in comparison to the fibres causes tensile residual stresses to form in the matrix and compressive stresses in the fibres. Macroscopic residual stresses can occur in composites at the same time as microscopic stresses, however, these occur mainly due to non-uniform shrinkage of different layers within the composite.

Due to the difficulty of assessing residual stresses, designers and engineers have often ignored them. However, this can be extremely dangerous as residual stresses can significantly reduce the life expectancy of the product, increasing the likelihood of warpage and in-service failure. In-service failures can include transverse cracking, deformation of non-symmetric laminates and reduced fatigue life. If the magnitude of the residual stress is unknown, higher safety factors must be used which will lead to overdesign of structures and increased weight.

1.1 CAUSES OF STRESSES

The development of residual stresses and distortions in composites occurs for a number of different reasons. The main causes are listed below [2]:

Thermal Expansion: The difference in the thermal expansion coefficients between the polymer matrix and the fibres produces tensile residual stresses in the matrix as the polymer contracts and compensating compressive stresses in the fibres. Furthermore, differences in the thermal expansion coefficients between the longitudinal and transverse directions of a composite can lead to residual stresses forming between plies or if the laminates are not correctly balanced to warpage.

Curing: Cross-linking of thermoset resins during the curing process can lead to an increase in density and the resulting shrinkage effects are similar to those that occur due to thermal expansion such as the formation of residual stresses or distortion. The difference between chemical and thermal residual stresses is that those caused by thermal effects will reduce as the temperature is increased, whereas chemical residual stresses are permanent.

Temperature Gradients: Rapid cooling of thick sections causes the surface of a composite to solidify significantly quicker than the core. Subsequent cooling will cause the core to solidify and shrink. However, shrinkage of the core will be constrained by the outer skin that is already solid. As a consequence, tensile residual stresses are formed at the centre of the component with large compressive stresses next to the surface.

Environmental Exposure: Residual stresses that develop during service are normally a consequence of environmental exposure. These can occur either due to fibre or matrix swelling due to the absorption of moisture or other chemical agents. Chemical surface treatments and coatings can also lead to the generation of substantial residual stress gradients close to the surface of components.

2 MEASUREMENT TECHNIQUES

A wide range of different techniques for the measurement of residual stress in composites have been proposed. The following section reviews the most promising of these techniques, giving some basic information about each technique, highlighting some of their key features, advantages and disadvantages. Tables summarising this information and allowing the different techniques to be compared are given in Appendices 1-3.

2.1 CURVATURE MEASUREMENTS

One of the simplest and most commonly used methods of determining the build-up of residual stresses in a composite material is through the measurement of curvature in an unbalanced composite laminate [3-6]. As each ply in a composite cools following manufacture it attempts to contract, primarily transverse to the direction of the fibres. If the composite is built-up of a symmetric series of cross-plies, the adjacent plies will constrain each other resulting in a build-up of residual stress. In an unbalanced cross-ply laminate this contraction is not constrained but results in curvature. By measuring the curvature that occurs in an unbalanced composite laminate and comparing it to the stresses predicted by modelling the laminate it is possible to predict the macroscopic residual stresses within each ply. The curvature of the specimen can be measured using a variety of different techniques including optical microscopy, profilometry, strain gauges and moiré interferometry [7-9]. The radius of curvature, ρ_c, can simply be determined from the height, h, and the length, L, of the strip (Figure 1), according to the following formula [6]:

$$h^2 - 2h\rho_c + \rho_c^2 \sin^2\left(\frac{L}{\rho_c}\right) \tag{1}$$

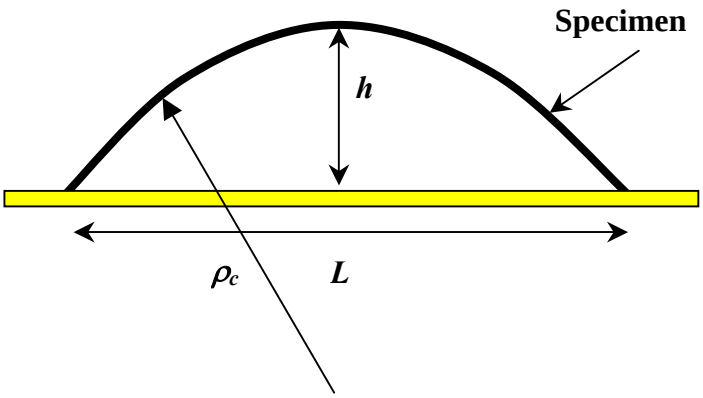

Figure 1: Determination of curvature in a composite strip.

The residual stresses that would exist in a symmetrical composite laminate can be calculated using classical lamination theories from the deformation that is observed in the unbalanced laminate. Knowledge of the longitudinal and transverse moduli E_{11} and E_{22} and the radius of curvature ρ_c at the test temperature are required to determine the residual stresses σ_r, using the following equation [6]:

$$\sigma_r = \frac{E_{11}E_{22}h}{\rho_c\left(E_{11}h + E_{22}k\right)}\left[\frac{b+d}{2} + \frac{E_{11}b^3 + E_{22}d^3}{6\left(b+d\right)}\left(\frac{1}{E_{11}b} + \frac{1}{E_{22}d}\right)\right] \tag{2}$$

Where, the thickness of the longitudinal and transverse plies in the unbalanced laminate are denoted by b and d, respectively while h and k are the corresponding ply thicknesses in the symmetrical lay-up.

The curvature method is simple and does not require highly specialist equipment or knowledge. It is, however, time consuming and can only give predictions for the macro-residual stresses within the composite.

2.2 LAYER REMOVAL

The layer-removal technique [10] is a relatively simple technique for the measurement of residual stresses in plates, which involves measuring the curvature of specimens following the progressive removal of thin layers from the surface. In response to removal of a layer the sample restores equilibrium by warping to a shape, which closely resembles a circular arc. The measured curvature as a function of depth can be used to calculate the stress distribution through the thickness of the sample prior to layer removal. The generalised relationship relating the bending moments (M_i) to the residual stresses (σ_i) is given by the following expression [11], the co-ordinates of which are given in Figure 2.

$$\sigma_x\left(z_1\right) = \frac{2}{z_0 + z_1}\frac{dM_x\left(z_1\right)}{dz_1} + \frac{2M_x\left(z_1\right)}{\left(z_0 + z_1\right)^2} - 4\int_{z_1}^{z_0}\frac{M_x\left(z\right)}{\left(z_0 + z\right)^3}dz \tag{3}$$

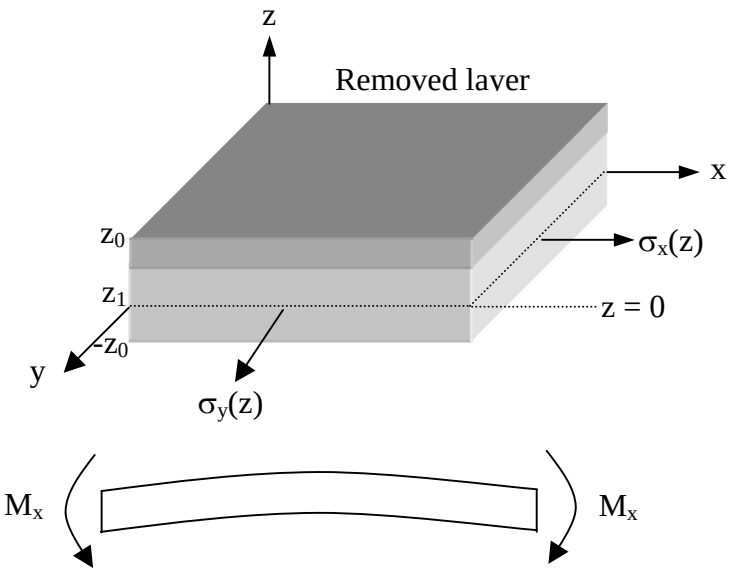

Figure 2 Co-ordinate system used in layer removal analysis [11]

An example of the variation in specimen deflection with progressive layer removal is shown for ABS in Figure 3.

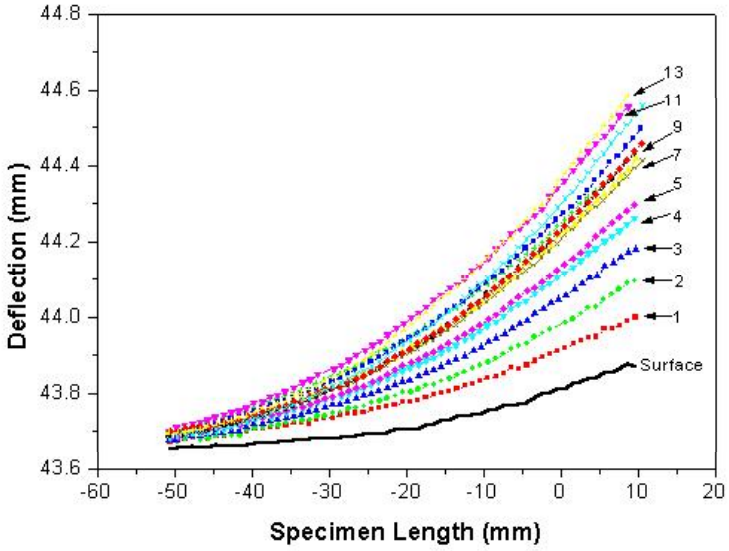

Figure 3: Deflection of a polymeric resin specimen during layer removal.

The technique has primarily been used for the measurement of residual stress in isotropic materials. However, Eijpe and Powell [12-14] have recently modified the layer removal analysis technique for the measurement of residual stress in cross-ply laminates. The authors have refined the technique to take into account extensional-bend coupling and variations in the mechanical properties through the thickness of the laminate. The limitation of the technique to essentially flat sheets is a major constraint as is the inability to assess very near-surface stresses. Furthermore, although the equipment required to make the measurements is relatively simple the technique is extremely time consuming and as a consequence costly.

2.3 COMPLIANCE TECHNIQUE

The compliance method is a powerful method capable of determining residual stress in materials as a function of depth. It has been used to determine residual stress in specimens of various geometries including cylinders [15], welded plates [16,17], and laser and shot-peened specimens [18], but has not been extensively used for the measurement of residual stress in composites [19]. The compliance method involves making thin cuts of progressively increasing depth into a composite to release the stresses along the plane of the cut and relating the resulting deformation to the residual stresses in the part before it was cut. A computational model is required to relate the deformation produced by the cutting process to the residual stresses that were in the material that has been removed. These relationships are known as compliance functions and can be obtained either experimentally using fracture mechanic solutions [16] or by using finite element analysis [17]. The compliance function can be obtained experimentally by applying a known load to a specimen and measuring the strains that are produced around the cut section. Once the compliance functions are known a slot can be cut into a specimen containing unknown levels of residual stress at incremental depths to release the stresses causing deformation. By measuring the strain next to the slot it is possible to determine the residual stresses at each depth within the material by using the compliance functions.

One specific application of the compliance technique is for the measurement of residual stresses in filament wound composite tubes. This application is more commonly called the slit-ring test [20-21]. It involves sectioning (Figure 4) the tubes and measuring the changes in the strains that occur on the walls of tube using biaxial strain gauges. This allows the axial and circumferential residual stresses in the tube to be determined.

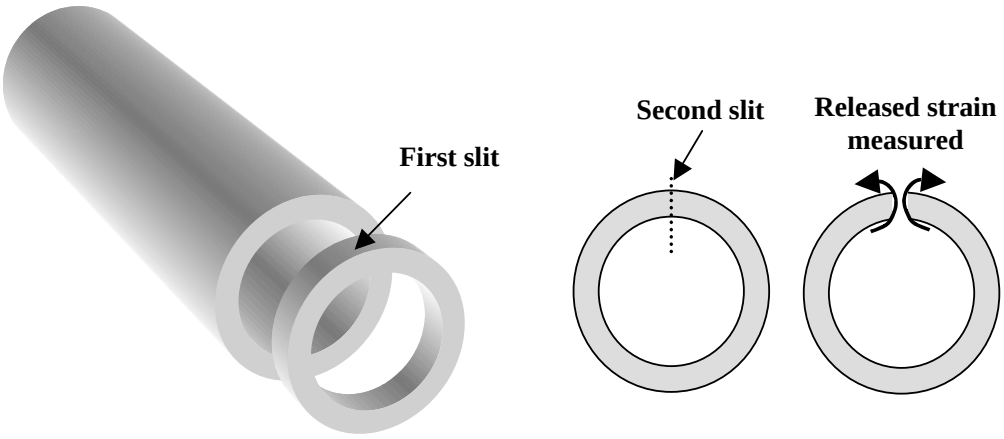

Figure 4: Slitting of filament wound tubes to determine residual stresses from bending moments.

The compliance method is, in principle, similar to the layer removal technique. The advantage of the compliance technique is that less material has to be removed to determine the residual stresses. This makes the compliance technique simpler to preform and less time consuming. The disadvantage of the technique is that the compliance functions that are required to convert the strains into stresses are considerably more complex.

2.4 HOLE DRILLING

Hole-drilling is widely used for the characterisation of residual stress in isotropic materials such as metals and ceramics [22] and has recently been applied to composites [23, 24]. The technique is, in principle, a compliance technique, which involves the drilling of a small hole into the surface of the component containing the residual stresses and measuring the deformation that occurs around the hole. The technique involves attaching a three-element strain-gauge rosette to the polymer surface to measure the strains (ε_1, ε_2 and ε_3) as the hole is drilled to varying depths through the centre of the rosette. The in-plane residual stresses can be calculated using the following equations for an isotropic material (Welywn Measurement Note 503-3) [25]:

$$\sigma_{\max} = \frac{\varepsilon_1 + \varepsilon_2}{4A} - \frac{\sqrt{2}}{4B}\sqrt{(\varepsilon_1 - \varepsilon_2)^2 + (\varepsilon_2 - \varepsilon_3)^2} \quad (4)$$

$$\sigma_{\min} = \frac{\varepsilon_1 + \varepsilon_2}{4A} + \frac{\sqrt{2}}{4B}\sqrt{(\varepsilon_1 - \varepsilon_2)^2 + (\varepsilon_2 - \varepsilon_3)^2} \quad (5)$$

where σ_{max} and σ_{min} are the maximum (most tensile) and minimum (most compressive) principal stresses present at the hole location before drilling. ε_1, ε_2, ε_3 are the relieved strains as measured by the correspondingly numbered, radially orientated strain gauges (Figure 5).

Schajer and Yang [26] have extended this method to orthotropic materials using the following equation to determine the residual stresses (σ_{11}, σ_{22}, σ_{33}) from the measured strains (ε_{11}, ε_{22}, ε_{33}):

$$\frac{1}{\sqrt{E_{xx}E_{yy}}}\begin{bmatrix} C_{11} & C_{12} & C_{13} \\ C_{21} & C_{22} & C_{23} \\ C_{31} & C_{32} & C_{33} \end{bmatrix}\begin{Bmatrix} \sigma_{11} \\ \sigma_{12} \\ \sigma_{22} \end{Bmatrix} = \begin{Bmatrix} \varepsilon_{11} \\ \varepsilon_{22} \\ \varepsilon_{33} \end{Bmatrix} \tag{6}$$

where E_{xx} and E_{yy} are the elastic moduli along the *x*- and *y*-axes and C_{11}-C_{33} are dimensionless coefficients. Schajer has calculated dimensionless coefficients for a wide range of different materials.

Residual stresses can be calculated to depths up to half the diameter of the hole using the incremental method [27]. However, it is extremely difficult to detect residual stresses in deep sections [28] or stresses that are very close to the surface. One of the main drawbacks to the use of the hole-drilling technique is the use of strain gauges as they can be difficult to attach to polymeric surfaces and movement of the gauges can easily distort the results. One possible method of overcoming this problem is to use digital imaging to record strain rather than strain gauges. Discrepancies can also arise during the drilling process due to either fibre pull-out or excessive heating. The technique is, however, quick and simple to use and is applicable to specimens of various geometries provided the area to be examined is flat enough to attach the strain gauges.

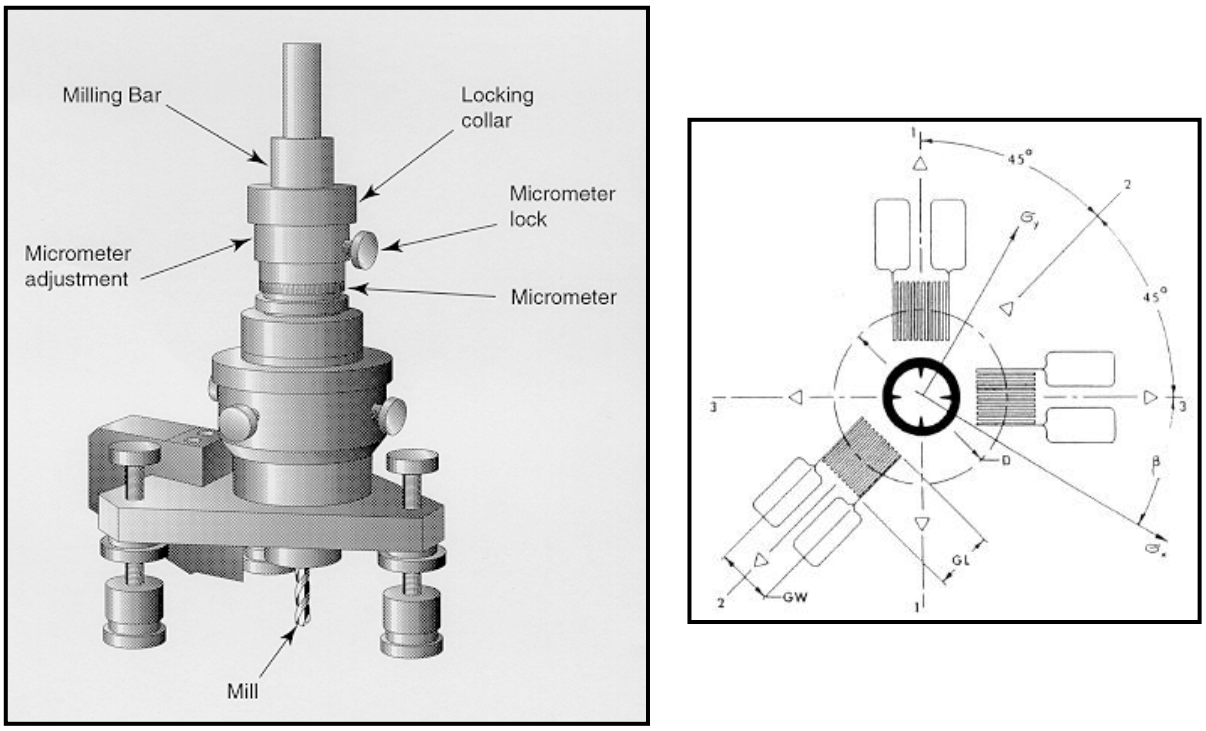

Figure 5: Conventional hole-drilling apparatus and strain-gauge arrangement [29].

2.5 CHEMICAL PROBE

The chemical probe technique involves establishing the stresses that are required to cause polymer specimens to crack or craze in different chemical environments and using this relationship to determine the magnitude of residual stress in components. This relationship is established by first annealing specimens of the polymer at a temperature high enough to remove any residual stresses from the material and then loading them at a known stress in a chemical environment. Stress can be applied to the specimens using either constant load as in a tensile test or constant strain as in a 4-point-bend test. This process is repeated using different stresses and chemical environments to establish the stress levels required to crack or craze the polymer in a range of chemicals (Figure 6). When a plastic with unknown residual stress is exposed for a specific period to one of these chemicals, the existence or otherwise of cracking or crazing will indicate whether the stress is above or below a particular value. This exercise is repeated for chemical environments of varying aggressivity in a progressive manner to estimate the magnitude of the residual stress in the polymer. The range of environments used is selected according to the accuracy of measurement required. A detailed discussion of the technique is given in the NPL Good Practice Guide on the measurement of residual stress in polymeric mouldings [29] and is similar to that of ASTM D 1939 which is specific to Acrylonitrile-Butadiene-Styrene (ABS). No information about stress distribution is obtained with this technique. The method is useful primarily for indicating near-surface tensile stresses. The technique is not constrained to specific geometries [31], although multi-axial residual stresses in complex components may create some uncertainty in the values.

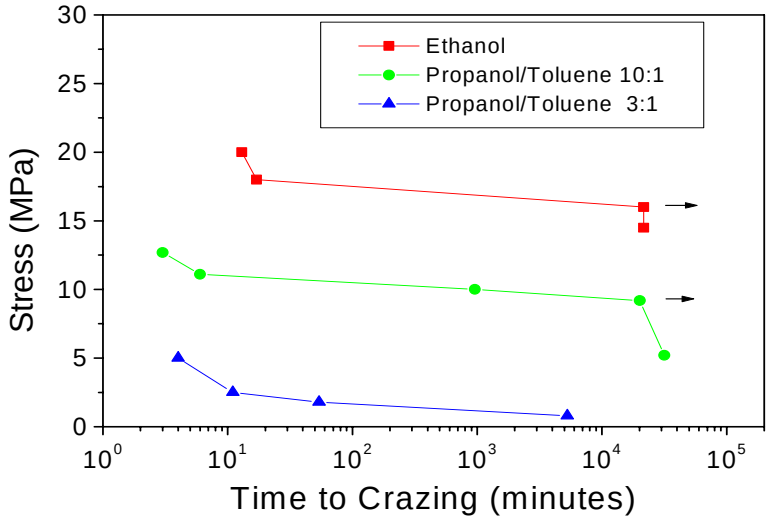

Figure 6: Chemical probe reference data establishing the relationship between the chemical treatment and the stress levels in the material [29].

2.6 PHOTELASTICITY

Optical polarizability of a polymer chain is anisotropic, that is the molecular backbone of the polymer has different polarizability in its longitudinal and transverse orientation. This anisotropy is determined by the chemical configuration and conformation of the chain. If the macromolecules are randomly coiled the anisotropy cancels out on a macroscopic scale. However, residual stress will result in distortion and will induce anisotropy of polarizability, which can then be determined by birefringence measurements [32]. The technique involves

viewing the interference fringe patterns that are obtained when the component to be examined is viewed with white or monochromatic light between two crossed polars. An example of the type of interference fringe patterns obtained is shown in Figure 7.

The stress distribution in the component can be obtained from the fringe patterns using the stress optic coefficient, n, that can be obtained from calibration experiments [33]:

$$\sigma_{11} - \sigma_{22} = \frac{fn}{t} \tag{7}$$

where σ_{11} and σ_{22} are the in plane principal stresses, f is the fringe order and t is the optical path length through the birefringent material.

The birefringence technique has obvious limitations for non-transparent materials and analysis in terms of residual stress is complicated due to ordering of molecular orientation induced by processing. The technique has, however, been applied to glass-fibre reinforced epoxy composites. Yan and Ohsawa [34] have used the technique to determine residual stress distribution in the epoxy resins around a single embedded glass-fibre and Pawlak and Galeski [35] developed a 3D technique for examining residual stresses around a spherical inclusion. The technique is mainly used for the quick, qualitative assessment of residual stress in transparent materials.

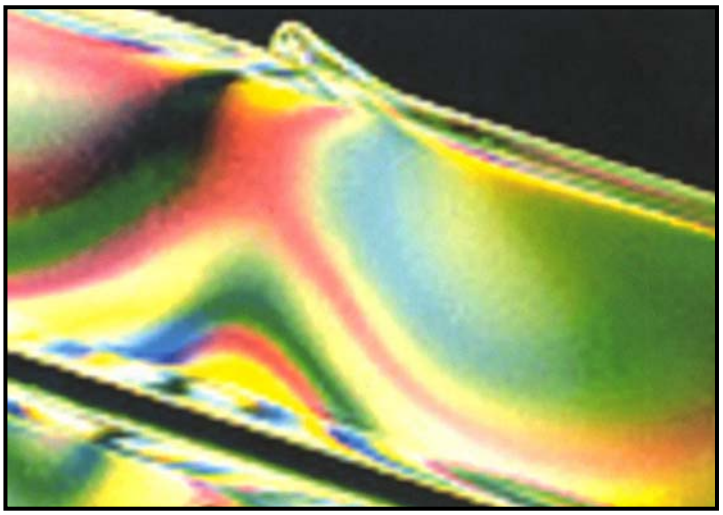

Figure 7: Birefringence patterns in a transparent plastic moulding.

2.7 X-RAY DIFFRACTION

Residual stresses in fibre composites can be determined using x-ray diffraction by doping the polymer resin with embedded metallic particles [36-40]. This technique relies on elastic deformations occurring within the embedded crystalline particles due to the presence of residual stresses within the polymer matrix. These elastic deformations cause changes in the spacing of the crystalline lattice of the metallic particles that are claimed to correspond to the stress in the material. Residual stress is measured by exposing a doped specimen to high energy x-rays that penetrate the surface of the material (Figure 8). The crystalline lattice within the metal particles diffracts a proportion of these x-rays according to Bragg's law. The intensity of the diffracted x-rays is monitored at different angular positions around the

specimen by moving a detector around the specimen. The location of these peaks enables the user to evaluate the stresses within the embedded metal particles.

The measurement technique is simple and the equipment easily available. However, the validity of the residual stresses obtained is uncertain as the embedded particles may alter the residual stress distribution within the composite. The strain in the particles will also depend on the bonding between the particles and the matrix.

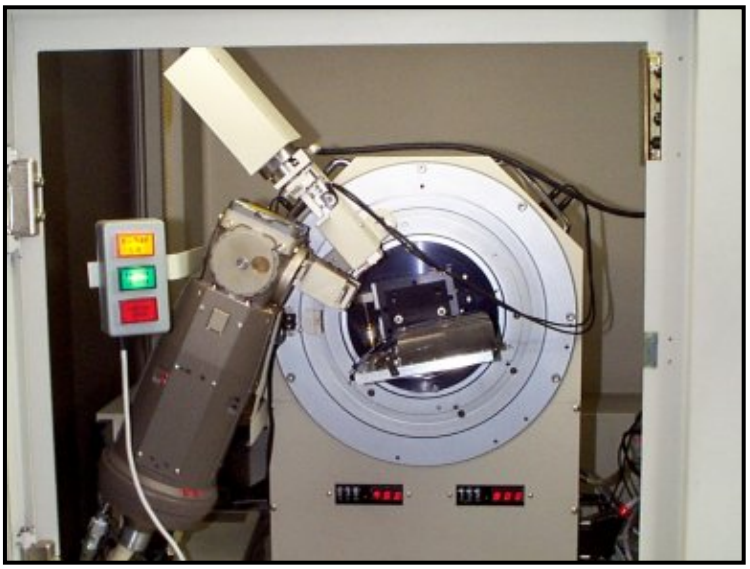

Figure 8: Typical x-ray diffraction apparatus showing the x-ray source, detector and goniometer [1].

2.8 RAMAN SPECTROSCOPY

Raman spectroscopy is based on the inelastic scattering of monochromic light from non-metallic materials. Laser light causes the bonds in the material to vibrate and by comparing the frequency of the scattered Raman light to the incident laser light it is possible to obtain information about the chemical and physical structure of the material [41-46]. Application of stress to a material will change the inter-atomic separation of its bonds, resulting in a corresponding change in the vibrational frequency of the bonds and hence a shift in the wavelength of peaks in the Raman spectra (Figure 9). This effect is particularly strong in crystalline materials and can be detected in both carbon or aramid fibres.

By loading individual fibres either in uniaxial tension or compression the magnitude of the shift in the Raman spectra can be measured. In general, compressive stresses will result in an increase in the Raman frequency and tensile stresses a reduction in the frequency [41]. This can be seen in Figure 9a for a single aramid fibre that has been subjected to an axial tensile deformation of 3% strain resulting in the wavelength of the Raman peak at 1610 cm^{-1} decreasing by approximately 10 cm^{-1}. This shift in the Raman peak has been shown to be linear with strain as demonstrated in Figure 9b. Furthermore, it has been shown that the frequency shift per unit stress is the same for all aramid fibres independent of the fibre modulus. It is therefore possible, provided no external stresses are applied to the composite, to determine the residual stresses in a carbon or aramid fibre directly from the shift in the Raman peaks.

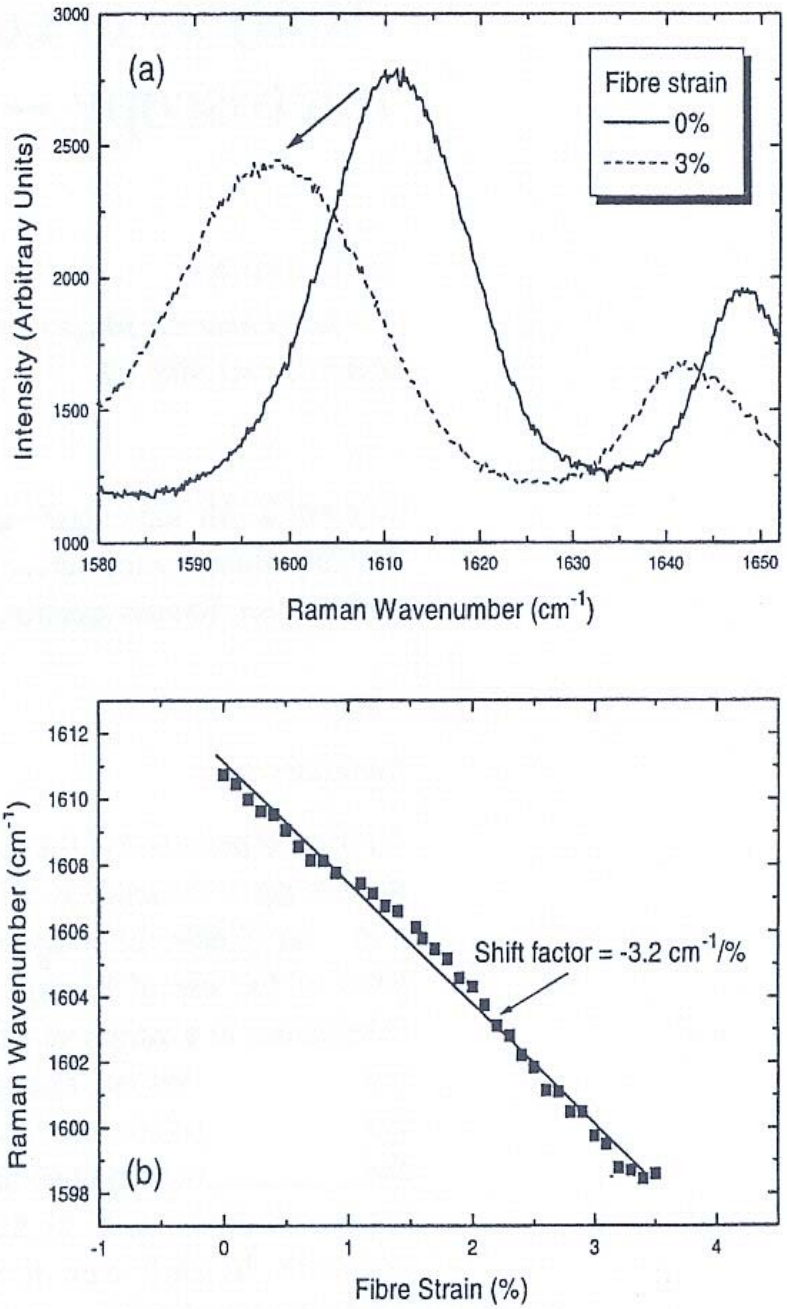

Figure 9: Effect of strain on the Raman spectrum of aramid composite fibre [41].

All carbon or aramid fibres situated near the surface of the composite can be interrogated remotely and non-destructively using this technique provided that the matrix is reasonably transparent. Fibres that are located in the bulk of a composite can be interrogated by means of a waveguide, such as a fibre optic cable, but in this case a certain amount of stress perturbation occurs. This method has a high spatial resolution (1 μm or less) and by using optical microscopy it is possible to select regions of interest just a few microns in size, allowing the stress distribution along fibres to be determined [43-46].

2.9 OPTICAL FIBRES

The most common fibre optic strain sensors available are: the extrinsic Fabry-Perot interferometer (EFPI) and the fibre Bragg grating (FBG). Whilst the EFPI is relatively insensitive to transverse strains and temperature changes, it is comparatively intrusive for embedding purposes [47] so FBGs are more commonly employed for residual strain measurements.

FBGs can be used as in-situ, real-time, non-destructive strain measuring devices in polymer composites. The fibres are small enough to introduce only minimal perturbation to the laminate microstructure and provide localised measurements of the cure, mechanical or residual stresses accumulated at selected locations within the component, with high sensitivity and good linearity [48-50]. It is possible to vary the position of these sensors, both within a ply and at different plies throughout a lay-up, to provide valuable information of the internal strain state particularly in thick composites [48, 51-52]. For example, within a unidirectional composite the strain measured in the transverse direction is significantly larger than that in the fibre-reinforced direction because the properties are matrix dominated and therefore exhibit large thermal and chemical deformations [50]. Mechanically the fibre acts as an elastic inclusion, so to obtain the correct strain and stress fields in the material under investigation may require micromechanical analysis between local strains and loading configuration, constituent materials, laminate architecture and the FBG interfacial bonding conditions affecting load transfer [52].

FBGs are typically single mode optical fibres with a short section of the length containing a spatially periodic modulation of the refractive index, which acts as a wavelength selective filter. They are manufactured by exposing the photosensitive fibre core to intense UV light and inscribing it using either a two-beam interference pattern or a phase-mask. They operate by strongly reflecting light from an incident broadband source over a narrow wavelength range, the Bragg wavelength, which is characterised by a finite bandwidth and a peak wavelength [47, 50, 53]. The Bragg wavelength is dependent on the effective refractive index of the core, n_{eff}, and the grating periodic spacing, Λ, shown in Figure 10.

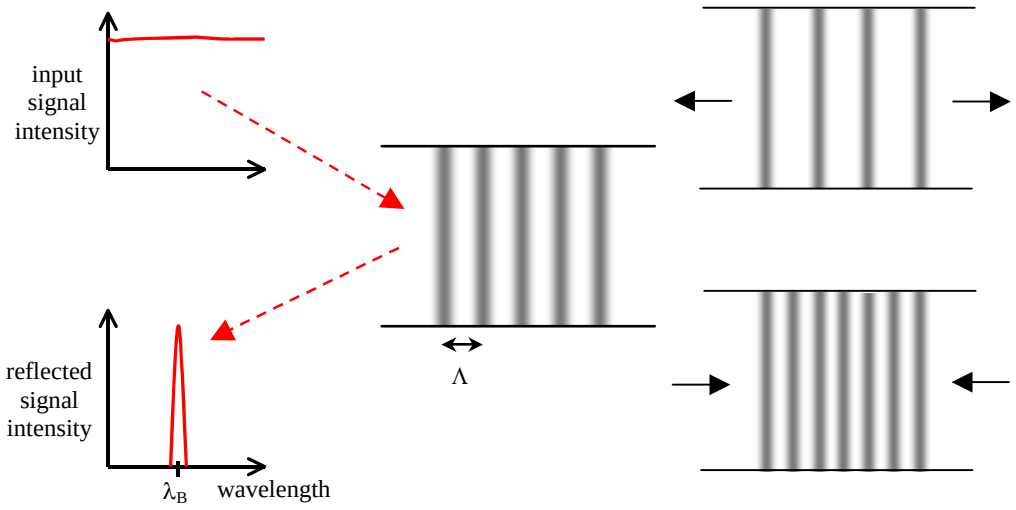

Figure 10: Typical spectral response of a fibre Bragg grating and the effect on the grating spacing of axial tension/compression.

The Bragg wavelength, λ_B, can be expressed as [50-51]:

$$\lambda_B = 2\, n_{eff} \Lambda \tag{8}$$

Consequently any external factors, i.e. mechanical strain, $\Delta\varepsilon$, or temperature, ΔT, which act to alter the characteristic grating properties can cause a shift in the reflected wavelength.

When uniform changes in strain or temperature occur, the FBG reflected spectral response exhibits a simple shift of the Bragg peak. Continuous monitoring therefore depends on tracking the wavelength position of the highest intensity peak in the reflection spectrum as it shifts with strain/temperature. For a 'free' fibre this wavelength shift can be expressed:

$$\Delta\lambda_B = \lambda_B \left(K\Delta\varepsilon + \beta\Delta T \right) \tag{9}$$

where K is the wavelength-strain sensitive factor (typically 1 pm/microstrain) and β is the wavelength-temperature sensitive factor (typically 10 pm/°C). Hence the influence of temperature is 10 times more significant than the effect of strain but the two effects cannot be separated with only one grating. This makes temperature measurement and compensation critical for accurate strain determination. In practice, the accuracy of the temperature subtraction depends on the precision of the temperature measurement device and its proximity to the FBG, as well as their relative response rates to temperature changes [49]. The sensitivity factors can be reduced further to:

$$K = 1 - p_e \tag{10}$$

$$\beta = \alpha_\Lambda + \zeta \tag{11}$$

where p_e is an effective strain-optic constant (given by $[1/2 n_{eff}^2 (p_{12} - \nu(p_{11} + p_{12}))]$ where ν is the Poisson's ratio of the fibre and p_{ij} are photoelastic constants) and $1-p_e$ is termed the gauge factor of the grating; α_Λ is the thermal expansion coefficient of the fibre/grating and ζ is the thermo-optic coefficient. In simplified terms, these factors make corrections to account for the following:

- strain-optic constant, p_e, - effect of mechanical strain on refractive index,
- thermal expansion coefficient, α_Λ, - effect of thermally induced strain on the grating period, and
- thermo-optic coefficient, ζ, - effects of <u>both</u> the thermal strain and the temperature on the refractive index.

A 'constrained' fibre, i.e. one which is embedded within a material, behaves as a 'free' fibre but with an additional contribution from the thermal expansion of the surrounding material. Hence, for a 'constrained' fibre:

$$\Delta\lambda_B = \lambda_B \left[K\Delta\varepsilon + \beta\Delta T + K\left(\alpha_s - \alpha_\Lambda\right) \right] \Delta T \tag{12}$$

where α_s is the coefficient of thermal expansion of the substrate or host material.

Generally, it is assumed that the strain thus determined is uniform along the grating and correlates to that particular location within the composite in the axial direction of the FBG. However, for most practical configurations, e.g. the consolidation of a multiaxial laminate, a non-uniform 3-D state of strain will exist around an FBG, which complicates the measurement and interpretation of the data. The presence of transverse strains induces birefringence in the fibre core, which may lead to the splitting of the initial single Bragg peak into two distinct ones (global Bragg shift still dependent on axial strain, ε_z). The peak wavelength separation, $\Delta\lambda_{By} - \Delta\lambda_{Bx}$, depends linearly on the difference between the two transverse components of strain, $\varepsilon_y - \varepsilon_x$, each of which are described by [52]:

$$\Delta\lambda_{B\,x,y} = \lambda_B \left[\varepsilon_z - 1/2 n_{eff} \left(p_{11}\varepsilon_{x,y} + p_{12}\left(\varepsilon_{y,x} + \varepsilon_z\right)\right) + \beta\Delta T \right] \quad (13)$$

Also, inhomogeneity in the axial strain field along the length of the FBG tends to broaden the spectral response and split it into multiple peaks, where each section of the grating effectively reflects different Bragg wavelengths (chirping), particularly evident in long gauge length FBGs [49,52,55]. The presence of other peaks in the reflection spectrum may introduce anomalous readings when their reflection intensities exceed that of the original measured peak (wavelength hopping) and ideally one would need to track the movement of the same peak throughout the process [53]. For this purpose an optical spectrum analyser (OSA) can help monitor disturbances to the spectrum and identify non-uniform strain effects [53-54].

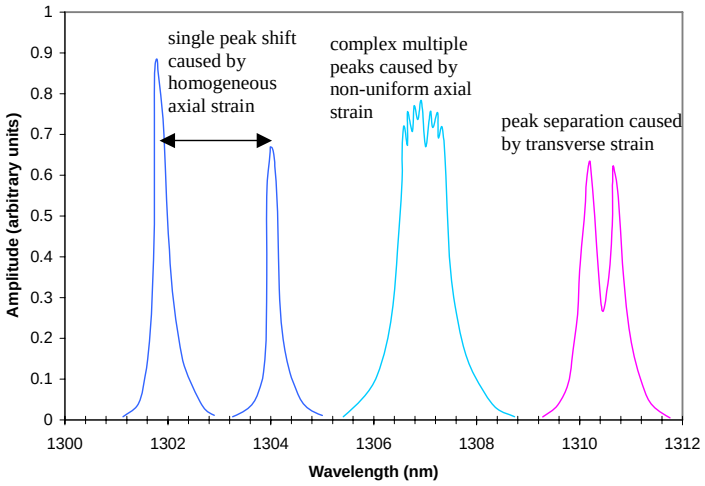

Figure 11: Typical spectral response of a fibre Bragg grating subjected to different non-uniform strain fields.

In practice, the optical fibre is stripped of its protective polymer coating (acrylic or polyimide), at least over the grating length, to improve bonding with the polymer matrix and because coatings can act to attenuate the effect of axial or transverse stress on the reflection spectrum [54]. This is placed into a composite lay-up, at known positions and orientations, usually parallel to the fibres in the ply to minimise disturbances. The fibre is passed through PTFE tubing as it exits the material to prevent fracture. Pre-strain may be applied to the fibre during the preparation stage to maintain straightness and position but this must be compensated for in subsequent strain calculations. The FBG signal is then captured using a simple peak wavelength detector or OSA. The simplest approach to determine residual strain is to measure the reflected spectrum of the fibre in the strain-free state before curing, after curing and after post curing [49, 52].

Alternatively, sensors can be monitored throughout the consolidation process [50] with post-manufacture measurements providing residual strain information since most residual strains develop during the cool-down period [48, 51] and when the laminates are de-moulded and free to expand/contract independently [49]. A typical strain profile is presented in Figure 12.

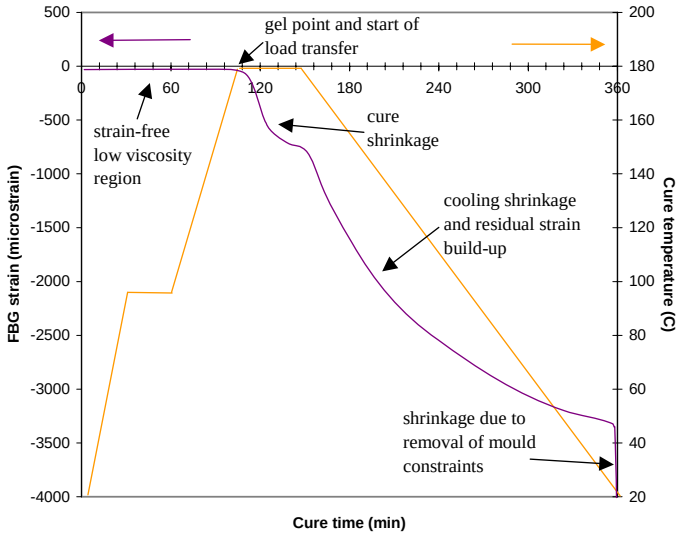

Figure 12: Temperature compensated strain profile monitored during and after composite cure showing the strain accumulation with respect to various stages of the cure schedule.

3 STRESS ANALYSIS

As fibre-reinforced composites are processed at elevated temperatures, thermal strains introduced during cure and cooling the composite material to room temperature may lead to residual stresses and changes in structural dimensions. These stresses are caused by a combination of matrix shrinkage during cure and differential thermal contraction between fibres and the polymer matrix (i.e. thermal expansion coefficient mismatch). This is further complicated by the differences in the fibre and matrix stiffness, distribution of fibres (i.e. lay-up) and fibre volume fraction. Differential thermal contraction and resin shrinkage produces tensile and compressive stresses in the resin and fibre, respectively. The magnitude of the resultant shear stress produced at the fibre-matrix interface in the as-cured composite can be a considerable percentage of the resin strength. Residual stresses can be sufficiently high to cause cracking and affect structural integrity (i.e. load-bearing capacity and life expectancy).

As shown in Section 2.1, a mismatch in thermal expansivity between adjacent laminae (or ply) of different fibre orientation within the laminate will result in residual thermal stresses and strains. Changes in structural dimensions can result in structural distortion, thus compromising design tolerance levels. This section considers classical laminate analysis as applied to continuous fibre-reinforced multidirectional laminates, concentrating on thermal expansion and the formation of residual stresses. It will consider key issues, such as stress-free temperature, non-linear thermal expansion behaviour with temperature and stress relaxation in laminates following cure.

3.1 LAMINATE ANALYSIS

In this section, the relevant relations required for the analysis of laminated composites consisting will be presented. The stress analysis will take into account the combined effect of mechanical and thermal loading [56-63].

The strains at any point in the laminate are related to the mid-plane strains ε^0_{xx}, ε^0_{yy} and ε^0_{xy} and plate curvatures κ_{xx}, κ_{yy} and κ_{xy} by [57-58]:

$$\begin{bmatrix} \varepsilon_{xx} \\ \varepsilon_{yy} \\ \gamma_{xy} \end{bmatrix} = \begin{bmatrix} \varepsilon^0_{xx} \\ \varepsilon^0_{yy} \\ \varepsilon^0_{xy} \end{bmatrix} + z \begin{bmatrix} \kappa_{xx} \\ \kappa_{yy} \\ \kappa_{xy} \end{bmatrix} \tag{14}$$

Superscript 0 denotes the mid-plane and z is the distance from the mid-plane (see Figure 13).

Stresses in the k_{th} lamina of a laminate can be determined using the following constitutive relation:

$$\begin{bmatrix} \sigma_{xx} \\ \sigma_{yy} \\ \tau_{xy} \end{bmatrix} = \left[\bar{Q}\right]_k \begin{bmatrix} \varepsilon^0_{xx} \\ \varepsilon^0_{yy} \\ \varepsilon^0_{xy} \end{bmatrix} + z \left[\bar{Q}\right]_k \begin{bmatrix} \kappa_{xx} \\ \kappa_{yy} \\ \kappa_{xy} \end{bmatrix} \tag{15}$$

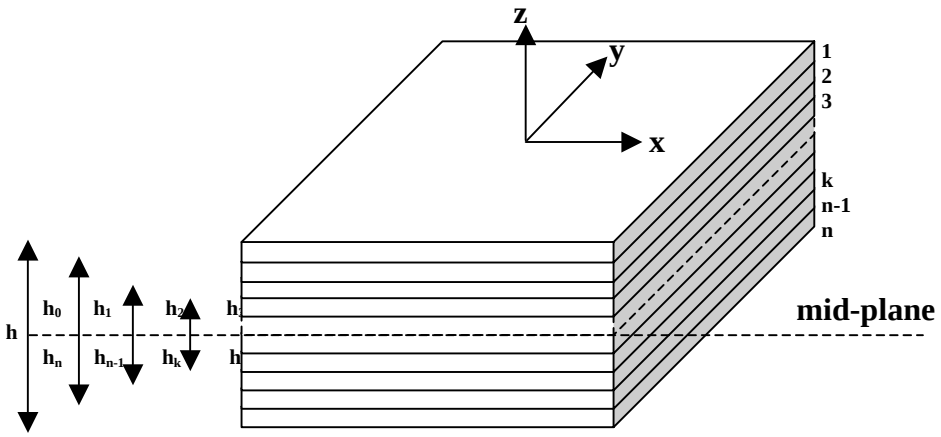

Figure 13: Laminate coordinate system.

The variation in stress through the laminate thickness can be obtained by calculating the stress variations in all the laminae (layers). It should be noted that the through-thickness variation in stress is generally non-linear. Stresses are in practice discontinuous at the interface between two laminae, and the gradient across two adjoining laminae is also different [57].

The transformed lamina stiffness matrix is defines as:

$$\left[\bar{Q}\right] = \begin{bmatrix} \bar{Q}_{11} & \bar{Q}_{12} & \bar{Q}_{16} \\ \bar{Q}_{12} & \bar{Q}_{22} & \bar{Q}_{26} \\ \bar{Q}_{16} & \bar{Q}_{26} & \bar{Q}_{66} \end{bmatrix} \tag{16}$$

The transformed lamina stiffness matrix terms are given below:

$$\begin{aligned} \bar{Q}_{11} &= Q_{11}m^4 + 2\left(Q_{12} + 2Q_{66}\right)m^2n^2 + Q_{22}n^4 \\ \bar{Q}_{22} &= Q_{11}n^4 + 2\left(Q_{12} + 2Q_{66}\right)m^2n^2 + Q_{22}m^4 \\ \bar{Q}_{12} &= \left(Q_{11} - Q_{22} - 4Q_{66}\right)m^2n^2 + Q_{12}\left(m^4 + n^4\right) \\ \bar{Q}_{66} &= \left(Q_{11} + Q_{22} - 2Q_{12} - 2Q_{66}\right)m^2n^2 + Q_{66}\left(m^4 + n^4\right) \\ \bar{Q}_{16} &= \left(Q_{11} - Q_{12} - 2Q_{66}\right)m^3n + \left(Q_{22} - Q_{12} - 2Q_{66}\right)mn^3 \\ \bar{Q}_{26} &= \left(Q_{11} - Q_{12} - 2Q_{66}\right)mn^3 + \left(Q_{22} - Q_{12} - 2Q_{66}\right)m^3n \end{aligned} \tag{17}$$

and $m = \cos\theta$ and $n = \sin\theta$ where θ is the fibre orientation with respect to the reference coordinate axes x-y (see Figure 14).

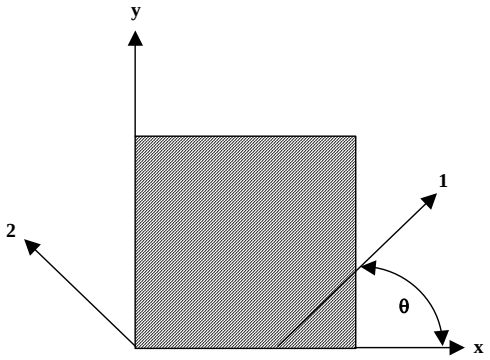

Figure 14: Rotation of principal material axes from reference coordinate system.

The lamina stiffness matrix terms Q_{11}, Q_{22}, Q_{12} and Q_{66} for a unidirectional lamina are related to the elastic constants as follows:

$$\begin{aligned} Q_{11} &= \frac{E_{11}}{\left(1 - \nu_{12}\nu_{21}\right)} \\ Q_{22} &= \frac{E_{22}}{\left(1 - \nu_{12}\nu_{21}\right)} \\ Q_{12} &= \frac{\nu_{12}E_{11}}{\left(1 - \nu_{12}\nu_{21}\right)} = \frac{\nu_{21}E_{22}}{\left(1 - \nu_{12}\nu_{21}\right)} \\ Q_{66} &= G_{12} \end{aligned} \tag{18}$$

E_{11}, E_{22} and G_{12} are the longitudinal, transverse and in-plane shear modulus, respectively. Elastic properties of the constituent laminae can either be determined using micromechanics equations or measured. Poisson's ratio ν_{12} corresponds to loading in the longitudinal direction and ν_{21} in the transverse direction. The minor Poisson's ratio ν_{21} is related to the major Poisson's ratio by the following relationship:

$$\nu_{21} = \nu_{12} \frac{E_{22}}{E_{11}} \tag{19}$$

The force-moment ***N-M*** system for an n-layered laminate can be determined by the summation of integrals representing the contribution of each layer as follows:

$$\begin{bmatrix} N_{xx} \\ N_{yy} \\ N_{xy} \end{bmatrix} = \sum_{k=1}^{n} \int_{h_{k-1}}^{h_k} \begin{bmatrix} \sigma_{xx} \\ \sigma_{yy} \\ \tau_{xy} \end{bmatrix} dz \tag{20}$$

$$\begin{bmatrix} M_{xx} \\ M_{yy} \\ M_{xy} \end{bmatrix} = \sum_{k=1}^{n} \int_{h_{k-1}}^{h_k} \begin{bmatrix} \sigma_{xx} \\ \sigma_{yy} \\ \tau_{xy} \end{bmatrix} z dz \tag{21}$$

The resultant forces N_{xx}, N_{yy} and N_{xy}, and resultant moments M_{xx}, M_{yy} and M_{xy} are related to the mid-plane strains ε^0_{xx}, ε^0_{yy} and ε^0_{xy} and plate curvatures κ_{xx}, κ_{yy} and κ_{xy} by:

$$\begin{bmatrix} N_{xx} \\ N_{yy} \\ N_{xy} \end{bmatrix} = \begin{bmatrix} A_{11} A_{12} A_{16} \\ A_{12} A_{22} A_{26} \\ A_{16} A_{26} A_{66} \end{bmatrix} \begin{bmatrix} \varepsilon^0_{xx} \\ \varepsilon^0_{yy} \\ \varepsilon^0_{xy} \end{bmatrix} + \begin{bmatrix} B_{11} B_{12} B_{16} \\ B_{12} B_{22} B_{26} \\ B_{16} B_{26} B_{66} \end{bmatrix} \begin{bmatrix} \kappa_{xx} \\ \kappa_{yy} \\ \kappa_{xy} \end{bmatrix} \tag{22}$$

$$\begin{bmatrix} M_{xx} \\ M_{yy} \\ M_{xy} \end{bmatrix} = \begin{bmatrix} B_{11} B_{12} B_{16} \\ B_{12} B_{22} B_{26} \\ B_{16} B_{26} B_{66} \end{bmatrix} \begin{bmatrix} \varepsilon^0_{xx} \\ \varepsilon^0_{yy} \\ \varepsilon^0_{xy} \end{bmatrix} + \begin{bmatrix} D_{11} D_{12} D_{16} \\ D_{12} D_{22} D_{26} \\ D_{16} D_{26} D_{66} \end{bmatrix} \begin{bmatrix} \kappa_{xx} \\ \kappa_{yy} \\ \kappa_{xy} \end{bmatrix} \tag{23}$$

where ε^0_{xx}, ε^0_{yy} and ε^0_{xy} are the mid-plane strains and κ_{xx}, κ_{yy} and κ_{xy} are the plate curvatures.

Extensional stiffness matrix [***A***], coupling stiffness matrix [***B***] and bending stiffness matrix [***D***] are given by:

$$A_{ij} = \sum_{k=1}^{n} \left(\bar{Q}_{ij} \right)_k \left(h_k - h_{k-1} \right) \tag{24}$$

$$B_{ij} = \frac{1}{2} \sum_{k=1}^{n} \left(\bar{Q}_{ij} \right)_k \left(h_k^2 - h_{k-1}^2 \right) \tag{25}$$

$$D_{ij} = \frac{1}{3}\sum_{k=1}^{n}\left(\bar{Q}_{ij}\right)_k \left(h_k^3 - h_{k-1}^3\right) \tag{26}$$

In general, normal forces applied to an arbitrarily oriented orthotropic lamina will produce shear strains in addition to the mid-plane normal strains. Similarly, a resultant shearing force will produce mid-plane normal strains in addition to shear strains. In the case of "balanced" laminate, the shear coupling stiffness components A_{16} and A_{26} vanish (i.e. $A_{16} = A_{26} = 0$). If the laminae within the laminate are positioned symmetrically about the laminate mid-plane, then all the components of the coupling stiffness matrix, [B], are equal to zero (i.e. $B_{ij} = 0$ for $i, j = 1, 2, 6$). It is important to note that while the in-plane shear and normal terms are uncoupled in the symmetric and balanced laminate, the twisting components of the bending stiffness matrix, [D], are non-zero (i.e. $D_{16}, D_{26} \neq 0$).

The constitutive relationships incorporating both thermal and mechanical loading can be written in terms of the extensional stiffness matrix [A] given by Equation (25), and the coupling stiffness matrix [B] and bending stiffness matrix [D]:

$$\begin{bmatrix} \bar{N} \\ \bar{M} \end{bmatrix} = \begin{bmatrix} A & B \\ B & D \end{bmatrix} \begin{bmatrix} \varepsilon \\ \kappa \end{bmatrix} \tag{27}$$

where:

$$\begin{aligned} \left[\bar{N}\right] &= \left[N\right] + \left[N^T\right] \\ \left[\bar{M}\right] &= \left[M\right] + \left[M^T\right] \end{aligned} \tag{28}$$

The effective thermal force and moment resultants due to thermal induced elastic deformations of the medium can be defined in terms of transformed lamina stiffness, $\bar{Q}_{ij}$, thermal expansion coefficients $\bar{\alpha}_{ij}$ and change in temperature, ΔT for the k_{th} lamina (see Figure 13) [56-63]:

$$\begin{aligned} N_{xx}^T &= \sum_{k=1}^{n}\left(\bar{Q}_{11}\bar{\alpha}_{11} + \bar{Q}_{12}\bar{\alpha}_{22} + \bar{Q}_{16}\bar{\alpha}_{66}\right)_k \left(z_k - z_{k-1}\right)\Delta T \\ N_{yy}^T &= \sum_{k=1}^{n}\left(\bar{Q}_{12}\bar{\alpha}_{11} + \bar{Q}_{22}\bar{\alpha}_{22} + \bar{Q}_{26}\bar{\alpha}_{66}\right)_k \left(z_k - z_{k-1}\right)\Delta T \\ N_{xy}^T &= \sum_{k=1}^{n}\left(\bar{Q}_{16}\bar{\alpha}_{11} + \bar{Q}_{26}\bar{\alpha}_{22} + \bar{Q}_{66}\bar{\alpha}_{66}\right)_k \left(z_k - z_{k-1}\right)\Delta T \end{aligned} \tag{29}$$

$$
\begin{aligned}
M_{xx}^{T} &= \frac{1}{2}\sum_{k=1}^{n}\left(\bar{Q}_{11}\bar{\alpha}_{11}+\bar{Q}_{12}\bar{\alpha}_{22}+\bar{Q}_{16}\bar{\alpha}_{66}\right)_k\left(z_k^2-z_{k-1}^2\right)\Delta T \\
M_{yy}^{T} &= \frac{1}{2}\sum_{k=1}^{n}\left(\bar{Q}_{12}\bar{\alpha}_{11}+\bar{Q}_{22}\bar{\alpha}_{22}+\bar{Q}_{26}\bar{\alpha}_{66}\right)_k\left(z_k^2-z_{k-1}^2\right)\Delta T \\
M_{xy}^{T} &= \frac{1}{2}\sum_{k=1}^{n}\left(\bar{Q}_{16}\bar{\alpha}_{11}+\bar{Q}_{26}\bar{\alpha}_{22}+\bar{Q}_{66}\bar{\alpha}_{66}\right)_k\left(z_k^2-z_{k-1}^2\right)\Delta T
\end{aligned}
\tag{30}
$$

where:

$$
\bar{\alpha}_{11} = \alpha_{xx}, \bar{\alpha}_{22} = \alpha_{xx}, \bar{\alpha}_{66} = \alpha_{xy}
\tag{31}
$$

The ply co-ordinates, z_k entered in Equations (30) and (31) may be calculated from the following recursion formulae:

$$
\begin{aligned}
z_k &= -h/2 \quad k=0 \\
zk &= z_{k-1} - h_k \quad k = 1,2,....,n
\end{aligned}
\tag{32}
$$

where h_k is the ply thickness of the k_{th} laminae.

The effective laminate thermal expansion coefficients for a balanced-symmetric laminates may be written in terms of the thermal force resultants, stiffness constants, A_{ij}, and ΔT (see below).

Longitudinal Thermal Expansion Coefficient:

$$
\alpha_{xx} = \frac{A_{22}N_{xx}^{T} - A_{12}N_{yy}^{T}}{\left(A_{11}A_{22}-A_{12}^2\right)\Delta T}
\tag{33}
$$

Transverse Thermal Expansion Coefficient:

$$
\alpha_{yy} = \frac{A_{11}N_{yy}^{T} - A_{12}N_{xx}^{T}}{\left(A_{11}A_{22}-A_{12}^2\right)\Delta T}
\tag{34}
$$

Shear Thermal Expansion Coefficient:

$$
\alpha_{xy} = \frac{N_{xy}^{T}}{A_{66}\Delta T} = 0
\tag{35}
$$

For a balanced symmetric laminate, α_{xx} and α_{yy} are principal coefficients of thermal expansion. In general, the shear thermal expansion coefficient, α_{xy} does not vanish.

For a simple cross-ply [0/90] (i.e. unsymmetric) laminate strip, the curvature κ can be calculated using the following approximation (see also Section 2.1) [64]:

$$
\kappa = \frac{1}{t}\left[\frac{24\left(E_{22}/E_{11}-\nu_{21}^2\right)\left(\alpha_{11}-\alpha_{22}\right)\Delta T}{1+14\left(E_{22}/E_{11}\right)+\left(E_{22}/E_{11}\right)^2-16\nu_{21}^2}\right]\left[\frac{1+E_{22}/E_{11}-2\nu_{21}}{1+E_{22}/E_{11}}\right]
\tag{36}
$$

Longitudinal and transverse thermal expansion coefficients α_{11} and α_{22} given in Equation (36) are defined in Section 3.2. ΔT is the temperature difference between the "stress-free temperature and ambient, and t is the laminate thickness.

The stress-free temperature, T_{sf}, is defined as the temperature at which stresses in a laminate with a thermosetting resin matrix begin to build-up [64-65]. This temperature is frequently assumed to be equivalent to the cure temperature. Actually it is lower, corresponding with the glass transition temperature T_g. The assumption that T_{sf} is equal to the cure-temperature will lead to overestimated residual stress values. The biaxial strip method described in Section 2.1 enables the measurement of T_{sf}. The temperature at which the strip becomes flat corresponds to the stress-free temperature. Thermal stress decreases approximately linearly with temperature and can attain values approaching the transverse tensile strength of the laminate [6]. For thermoplastics, these assumptions do not apply. Stress build-up will not necessarily commence upon cool down, but may occur at the onset of crystallisation or at the glass transition. The value of T_{sf} is dependent on the material and rate of cooling [65].

A second difficulty in estimating residual stresses is caused by stress relaxation that occurs during cooling and post-cure. Neglecting stress relaxation in the calculations will overestimate residual stresses [6, 65-66]. Stress relaxation can be expected to be significant for thermoplastic-based composite systems. Residual stresses can be predicted with reasonable accuracy using classical laminate analysis provided the relations between thermal expansion coefficients and elastic constants and temperature are known. Moisture absorption needs to be considered as it can have a dual effect on residual stress (i.e. plasticization and swelling of the matrix).

3.2 LAMINAE THERMAL EXPANSION COEFFICIENTS

Unidirectional laminae have two principal thermal expansion coefficients, longitudinal expansion coefficient, α_{11c}, and transverse expansion coefficient, α_{22c}. Since the longitudinal thermal expansion coefficient of fibres, α_{11f}, is generally small in comparison with the expansion coefficient of the matrix material, α_m, it can be expected that the resultant expansion coefficient of the lamina, α_{11c}, is also small (i.e. comparable in magnitude to α_{11f}). In contrast, the transverse thermal expansion coefficient, α_{22c} of the composite can be greater than the unreinforced matrix material for low fibre volume fractions. This is because the matrix is restrained from fully expanding along the fibre direction of the lamina and is forced to expand in the transverse direction to a greater extent than normally encountered in the unreinforced state [57, 60].

Hashin [67-68] derived linear longitudinal and transverse thermal expansion coefficients for the case of continuous orthotropic fibres. The longitudinal thermal coefficient can be approximated by:

$$\alpha_{11c} = \frac{E_{11f}\alpha_{11f}V_f + E_m\alpha_m V_m}{E_{11f}V_f + E_m V_m} \tag{37}$$

and the transverse thermal coefficient can be calculated using:

$$\alpha_{22c} = \alpha_m V_m (1+\nu_m) + \alpha_{22f} V_f (1 + \nu_{12f}\alpha_{11f}/\alpha_{22f}) - \alpha_{11c}(\nu_{12f}V_f + \nu_m V_m) \tag{38}$$

E_{11f} is the fibre longitudinal modulus, E_m is the Young's modulus of the matrix, ν_m is the Poisson's ratio of the matrix, and V_f and V_m are fibre and matrix volume fractions, respectively. These equations are similar to those developed by Schapery [69] for unidirectional lamina with isotropic constituents. It is assumed in the micromechanics analysis that the thermal expansion coefficients are constant over temperature range that fibre-reinforced plastics normally operate. In fact for most fibres, polymers and thus fibre-reinforced composite materials, thermal expansion coefficients are temperature dependent [57].

4 SUMMARY

The most widely used technique for the measurement of residual stress in composites is the curvature technique. This involves measuring the curvature of an unsymmetric laminate and using this measurement to predict the residual stresses that are present in a similar symmetric laminate. This technique is simple and does not require highly specialist equipment or knowledge. It can, however, only be used to predict the macro-residual stresses within the composite.

A technique that is widely used for measuring residual stress in metals and ceramics is the hole-drilling method. This involves drilling a small hole into the surface of the component and measuring the deformation that occurs around the hole. The technique is quick and simple to use and capable of measuring localised values of residual stress. It has, however, only recently been applied to composites due to the difficulty in relating the measured strains to the residual stresses in an anisotropic material such as a composite.

Residual stress values can be obtained from carbon or aramid fibres by measuring the strain using Raman spectroscopy. This technique has the advantage of having high spatial resolution and can be used to examine regions of just a few microns in size. The main limitation is that it cannot be used on glass fibre-reinforced composites.

Recently, Bragg fibre optical sensors have been used to determine information relating to strain fields that develop in composites during curing. These tiny sensors can be embedded into the body of the composite, with minimum effect on the strain field between the fibre and the resin. The advantage of these techniques is that they can potentially be used for on-line and in-service monitoring of residual stresses.

Other methods that have been explored as feasible techniques for characterising the residual stress in composites include; layer removal, chemical probe, photoelasticity and X-ray analysis. These techniques are, however, of limited use. Layer removal is limited to flat sheets, the chemical probe is only capable of measuring residual stress in the surface resin, photoelasticity can only be used for transparent birefringent resins and X-ray analysis can only be used in composites specially doped with metallic particles.

Attempts at modelling the formation of residual stresses in composites using laminate analysis have been shown to give results that are consistent with values obtained using the curvature method. However, further research is required to demonstrate the validity of this model.

5 RECOMMENDATIONS

The key recommendations of this review are to:

1) Produce a series of carbon/epoxy laminates for assessing residual stress in composites, including both symmetric (**s**) and unsymmetric laminates. The symmetric laminates including both "blocked" and "distributed" plies:
   - Blocked plies $[+45_n/-45_n/0_n/90_n]_s$
   - Distributed plies $[+45/-45/0/90]_{ns}$ where **n** = 1, 2, 3, 4

2) Conduct a feasibility study to assess the most promising measurement techniques that were identified in the review, this should include:
   - Curvature measurements
   - Hole-drilling
   - Raman spectroscopy
   - Embedded optical fibres

3) Demonstrate the feasibility of using laminate analysis to predict the formation of residual stresses in symmetric and unsymmetric laminates. This will include obtaining experimental data to define the:
   - Elastic properties as a function of temperature (E_{11}, E_{22}, G_{12}, ν_{12}, ν_{21})
   - Thermal expansion coefficients as a function of temperature (α_{11}, α_{22})
   - Stress free temperature

   The modelling needs to take into account the effects of "blocked" and "distributed" plies, and stress relaxation that occurs following cure.

ACKNOWLEDGEMENTS

This work was funded by the United Kingdom Department of Trade and Industry (National Measurement System Policy Unit) as part of the Measurements for Materials Characterisation programme.

REFERENCES

1 Kandil F., Lord J., Fry A. and Grant P. "A Review of Residual Stress Measurement Methods, NPL Report MATC (A) 04 (2001).
2 Wisnom M.R. and Potter K.D., "Mechanisms Generating Residual Stresses and Distortion During Manufacture of Polymer Matrix Composite Structures", Proceedings of Euromech 453, St. Etienne, France 2003.
3 Djokic D., Johnston A., Rogers A., Lee-Sullivan P. and Mrad N.," Residual Stress Development During the Composite Patch Bonding Process: Measurement and Modelling", Composites Part A: Applied Science and Manufacturing 33A (2002) pp 277-288.
4 Youssef Y. and Denault J., " Thermoformed Glass Fibre Reinforced Polypropylene: Microstructure, Mechanical Properties and Residual Stresses", Polymer Composites 19 (1998), pp 301-9.
5 Kim K. S. and Hahn H. T., "Residual Stress Development During Processing of Graphite/Epoxy Composites", Composites Science and Technology 36 (1989), pp 121-132.
6 Cowley K. D. and Beaumont P. W. R., "The Measurement and Prediction of Residual Stresses in Carbon-Fibre/Polymer Composites", Composites Science And Technology 57 (1997), pp 1445-1455.
7 Ifju P. G., Kilday B. C., Niu X. and Liu, S-C., "Proceedings- American Society for Composites" American Society for Composites, 12 (1997), pp 1141-1150.
8 Ifju P.G., Kilday B.C., Niu X. and Liu S, "A Novel method to Measure Residual Stresses in Laminated Composites", Journal of composite materials, 33 (1999), pp 1511-1524.
9 Schulz W. A., Myers, D.G., Singer T.N., Ifju P.G. and Haftka R. T., "Determination of Residual Stress and Thermal History for IM7/977-2 Composite Laminates", Composite Science and Technology, 65 (2005), pp 2014-2024.
10 Hindle C.S., White J.R., Dawson D. and Thomas K., "Internal stress molecular Orientation and Distortion in Injection Moldings, Polypropylene and Glass-fibre filled Polypropylene", Polymer Engineering and Science, 32 (1992), pp 157-171.
11 Treuting R.G. and Read W.T., "A Mechanical Determination of Residual Stresses in Sheet Materials", J. Appl. Phys. **22** (1951), pp 130-134.
12 Eijpe, M. P. I. M. and Powell, P. C., " Residual Stress Evaluation in Composites Using a Modified Layer Removal Method", Composite Structures - Barking - 1997 Vol 37; Number 3/4, pp 335-342.
13 Eijpe M. P. I. M. and Powell P C., "Determination Of Residual Shear Stresses In Composites By A Modified Layer-Removal Method", Journal of Materials Science 33 (1998), pp 2019-26.
14 Eijpe M. P. I. M. and Powell P C., "Modified Layer Removal Analysis For Determination Of Internal Stresses In Polymer Composites", Journal of Thermoplastic Composite Materials, 10 (1997), pp 334-52.

15 Fett, T. and Thun, G., "Residual Stresses in PVC-Cylinders Determined with the Weight Function Method", Engineering Fracture Mechanics, 55 (1996), pp 859-863.
16 Kang, K.J., Song J.H. and Earmme, Y.Y., "A Method for the Measurement of Residual Stresses using a Fracture Mechanics Approach", Journal of Strain Analysis, 24 (1989), pp 23-30.
17 Beghini, M. and Bertini L., "Residual Stress Modelling by Experimental Measurements and Finite Element Analysis", Journal of Strain Analysis for Engineering Design, 25 (1990), pp 103-108.
18 Cheng, W., Finnie I., Gremaud, M., Rosselet A. and Streit R.D., "The Compliance Method for the Measurement for Near Surface Residual Stresses – Application and validation for Surface Treatment by Laser and Shot-Peening", Journal of Engineering Materials and Technology, 116 (1994), pp 556-560.
19 Ersoy N. and Vardar O., "Measurement of Residual Stress in Layered Composites by Compliance Method", Journal of Composite Materials Vol 34, No7 (2000), pp 575-598.
20 Tzeng J T., "Predictions and Experimental Verification of Residual Stresses in Thermoplastic Composite Cylinders", Journal of Thermoplastic Composite Materials 8 (1995), pp 163-79.
21 Casari P., Jacquemin F. and Davies P., "Characterisation of Residual Stresses in wound Composite Tubes", Composites: Part A 37 (2006), pp 337-343.
22 ASTM E 837-94a, "Determining Residual Stresses by the Hole-drilling Strain-Gage Method".
23 Shokrieh M. M. and Kamali S. M., "Theoretical and Experimental Studies on Residual Stresses in Laminated Polymer Composites", Journal of Composite Materials 39 (2005), pp 2213-2225.
24 Sitcot O., Gong X. L., Cherouat A. and Lu J., "Determination of Residual Stress in Composite Laminates Using the Incremental Hole-Drilling Method", Journal of Composite Materials, 37 (2003), pp 831-844.
25 "Residual Stress Measurement", TN-503-3, Welwyn Strain Measurement, Measurement Group Inc. (1988).
26 Schajer G.S. and Yang L., "Residual-Stress Measurement in Orthotropic Materials Using the Hole-drilling Method", Experimental Mechanics, 12 (1994), pp 324-333.
27 Sicot O., Gong X. L., Cherouat A. and Lu J. "Measurement of Residual Stress in Composite laminates using the Incremental Hole-drilling Method", journal of Composite Materials, 37 (1996), pp 575-598.
28 Schajer G. S. and Altus E., "Stress Calculation Error Analysis for Incremental Hole-drilling residual Stress Measurements", Journal of Engineering Materials and Technology", 118 (1996), pp 120-126.
29 Turnbull A., Maxwell A. S., Pillai S. and White J., "The Measurement of Residual Stress in Polymeric Mouldings", NPL Good Practice Guide No. 10, National Physical Laboratory, Teddington, UK, 1998.
30 ASTM D 1939, "Determining Residual Stresses in Extruded or Molded Acrylonitrile-Butadiene-Styrene (ABS) Parts by Immersion in Glacial Acetic Acid".
31 Maxwell A.S. and Turnbull A., "Chemical Probe Technique for Assessing the Susceptibility of Polymeric Mouldings to Environment Stress Cracking", Polymer Testing, 22 (2003), pp 259-265.
32 ASTM D 4093, "Standard Test Method for Photoelastic Measurements of Birefringence and Residual Strains in Transparent or Translucent Plastic Materials".
33 Patterson E.A., "Encyclopedia of Material Science and Technology" ed. Buschow K. H, J., Oxford Press (2001).

34 Yan X. and Ohsawa T., "Measurement of The Internal Local Stress Distribution of Composite Materials by Means of Laser Imaging Methods", Composites 25 (1994), pp 443-450.

35 Pawlak A. and Galeski A., " Residual Stresses in Epoxy Systems by 3-D Photoelastic Method", Polymer Engineering and Science, 36 (1996), pp 2727-2735.

36 Meske R. and Schnack E.,"Particular Adaptation of X-ray Diffraction to Fiber Reinforced Composites", Mechanics of Materials, 35 (2003) pp 19-34.

37 Benedikt B.; Gentz M.; Kumosa L.; Rupnowski P.; Sutter J. K.; Predecki P. K. and Kumosa M, "X-Ray Diffraction Experiments on Aged Graphite Fiber/Polyimide Composites with Embedded Aluminum Inclusions", Composites Part A: Applied Science and Manufacturing 35A (2004), pp 667-681.

38 Benedikt B.; Predecki P.; Kumosa L.; Armentrout D.; Sutter J. K. and Kumosa M., "Use of X-Ray Diffraction Measurements to Determine the Effect of Bending Loads on Internal Stresses in Aluminium Inclusions Embedded in Unidirectional Graphite-Fibre/PMR-15 Composite", Composites Science and Technology 61 (2001), pp 1995-2006.

39 Benedikt B.; Kumosa M.; Predec P. K.; Kumosa L.; Castelli M. G. and Sutter J K., "Analysis of Residual Thermal Stresses in Unidirectional Graphite/PMR-15 Composite Based on X-Ray Diffraction Measurements", Composites Science and Technology, 61 (2001), pp 1977-1994.

40 Fenn R. H; Jones A. M, and Wells G. M., "X-Ray Diffraction Investigation of Triaxial Residual Stress in Composite Materials", Journal of Composite Materials, 27 (1993), pp 1338-1351.

41 Young R. J., " Analysis of Composites using Raman and Fluorescence Microscopy - A Review", J. of Microscopy, 185 (1997), pp 199-205.

42 Colomban P., Gouadec G., Mathez J., Tschiember J. and Peres P., "Raman Stress Measurement in Opaque Industrial Cf/Epoxy Composites Submitted to Tensile Strain", Composites Part A 37 (2006), pp 646-651.

43 Nielsen A. S. and Pyrz R., "Raman Study into the Effect of Transcrystallisation on Thermal Stresses in Embedded Single Fibres", Journal of Materials Science 38 (2003), pp 597-601.

44 Nielsen A. S. and Pyrz R., " Study of the Influence of Thermal History on the Load Transfer Efficiency and Fibre Failure in Carbon/Polypropylene Microcomposites Using Raman Spectroscopy", Composite Interfaces 6 (1999), pp 467-482.

45 Heppenstall-Butler M. and Young R. J., "Investigation of Axial Fibre Stresses in Transcrystalline Regions of Single-Fibre Aramid/Polypropylene Composites Using Raman Spectroscopy", Journal of Materials Science Letters 14 (1995), pp 1638-40.

46 Filiou C.; Galiotis C. and Batchelder D. N., "Residual Stress Distribution in Carbon Fibre Thermoplastic Matrix Pre-Impregnated Composite Tapes", Composites 23 (1992), pp 28-38.

47 Lawrence C., Nelson D., Spingarn J. and Bennett T., “Measurement of process-induced strains in composite materials using embedded fibre optic sensors”, Proceedings of SPIE 2718 (1996), pp 60-68.

48 Kang H., Kang D., Bang H., Hong C. and Kim C., “Cure monitoring of composite laminates using fibre optic sensor”, Smart Materials and Structures 11 (2002), pp 279-287.

49 Sorensen L., Gmür T. and Botsis J., “Long FBG sensor characterisation of residual strains in AS4/PPS thermoplastic laminates”, Proceedings of SPIE 5384 (2004), pp 267-278.

50 Lodeiro M. J. and Mulligan D. R. “Cure monitoring techniques for polymer composites, adhesives and coatings”, NPL Measurement Good Practice Guide no. 75 (2005).

51 Leng J. and Asundi A., “Real-time cure monitoring of smart composite materials using extrinsic Fabry-Perot interferometer and fibre Bragg grating sensors”, Smart Materials and Structures 11 (2002), pp 249-255.

52 Botsis J., Humbert L., Colpo F. and Giaccari P., “Embedded fibre Bragg grating sensor for internal strain measurements in polymeric materials”, Optic and Lasers in Engineering 43 (2005), pp 491-510.

53 Kuang K., Kenny R., Whelan M., Cantwell W. and Chalker P., “Embedded fibre Bragg grating sensors in advanced composite materials”, Composites Science and Technology 61 (2001), pp 1379-1387.

54 Okabe Y., Yashiro S., Tsuji R., Mizutani T. and Takeda N., “Effect of thermal residual stress on the reflection spectrum from fibre Bragg grating sensors embedded in CFRP laminates”, Composites Part A (2002), pp 991-999.

55 Menendez J. and Guemes J., “Bragg grating-based multiaxial strain sensing: its application to residual strain measurement in composite laminates”, Proceedings of SPIE 3986 (2000), pp 271-281.

56 Jones R. M., “Mechanics of Composite Materials”, McGraw-Hill, New York, (1975).

57 Argwal B. D. and Broutman L. J., “Analysis and Performance of Fiber Composites", John Wiley and Sons, New York (1980).

58 Ashton J.E., Halpin, J.C. and Petit, P.H., “Primer of Composite Materials analysis”, Technomic Publishing Company, Inc., Standford, Conneticut, USA, 1980.

59 Tsai S.W. and Hahn H. T., “Introduction to Composite Materials”, Technomic Publishing Company, Inc, Westport, Conneticut, USA, (1980).

60 Hull D., “An Introduction to Composite Materials”, Cambridge University Press, Cambridge, UK (1981).

61 Tsai S. W., “Composites Design”, Third Edition, Think Composites, Dayton, Ohio, USA, (1987).

62 Datoo M.H., “Mechanics of Fibrous Composites”, Elsevier applied science, (1991).

63 Eckold, G., “Design and Manufacture of Composite Structures”, Woodhead Publishing Limited, (1994).

64 Kim K. S. and Hahn H. T., “Residual Stress Development During Processing of Graphite/Epoxy Composites”, Composites Science and Technology 36 (1989), pp 121-132.

65 Jeronimidis G. and Parkyn A. T., “Residual Stresses in carbon Fibre-Thermoplastic Matrix laminates”, Journal of Composite Materials 22 (1988), pp 401-415.

66 Chapman T. J., Gillespie Jr J. W., Pipes R. B. Manson J-A. E. and Seferis J. C., “Prediction of Process-Induced Residual Stresses in Thermoplastic Composites”, Journal of Composite Materials 24 (1990), pp 616-643.

67 Hashin Z., "Analysis of Properties of Fiber Composites with Anisotropic Constituents", Journal of Applied Mechanics, Vol 46, No 3 (1979), pp 543-550.

68 Whitney J.M., and Daniel I. M. and Pipes R.B., "Experimental Mechanics of Fiber Reinforced Composite Materials", Society for Experimental Stress Analysis Monograph No.4, Brookfield Centre, Conneticut (1982).

69 Schapery J., "Thermal Expansion Coefficients of Composite Materials Based on Energy Principles", Journal of Composite Materials, 2 (1968), pp 380-404.

Appendix 1 Summary of Measurement Techniques

Techniques	Type of component	Contact or non-contact	Destructive	Lab-based or portable	Speed	Cost of Equipment	Cost of measurement	Level of expertise required
Curvature	Flat sheets	Contact	No	Lab	Med	Low	Med	Low/Med
Layer removal	Flat sheets	Contact	Yes	Lab	Med	Low	Med/High	Low/Med
Compliance	Unbalanced laminates	Contact	Yes	Both	Fast	Low	Med	Low/Med
Hole-drilling	Component surfaces	Contact	Yes	Both	Fast/med	Low/Med	Low	Low/Med
Chemical probe	Component surfaces	Contact	Yes	Both	Fast	Low	Low	Low
Photoelasticity	Transparent components	Non-contact	No	Both	Fast	Low	Low	Low
X-ray	Metal doped matrix required	Non-contact	No	Lab	Med	High	Med	Med/High
Raman	Carbon or Kevlar fibres	Non-contact	No	Both	Fast	Med/high	Med/Low	Med
Optical fibres	Embedded optical fibres	Contact	No	Both	Fast	Med	Low	Med

Appendix 2 Physical Capabilities of Techniques

Techniques	Resolution	Penetration	Stress gradient	Sampling area	Sample preparation required
Curvature	Ply thickness	Whole specimen	No	Whole specimen, one ply thick	Unsymmetrical specimen required
Layer removal	Thickness of layer removed	Whole specimen	Yes	Whole specimen, one layer thick	Remove layer
Compliance	1 mm	Thickness of pipe	Yes	Thickness of pipe along slit	Cut pipe
Hole-drilling	50-100 μm depth increments	Hole diameter	Yes but difficult to interpret	1-2 mm diam. 1-2 mm deep	Fix strain gauge and drill hole
Chemical probe	1 mm	Surface only	No	Whole specimen surface	Apply chemical
Photoelasticity	1 mm	Transparent materials only	No	Whole specimen surface	None
X-ray	20 μm	0.1 mm	Only combined with layer removal	1-2mm lateral 0.1 mm deep	Embed metal particles
Raman	0.5 μm	Along fibre	Yes (by examining different fibres)	Fibre area	None
Optical fibres	100 μm	Along fibre	Yes (by examining different fibres)	Fibre area	Embed fibres

Appendix 3 Advantages and Disadvantages of Tests

Techniques	Advantages	Disadvantages
Curvature	• Relatively simple • Non-destructive	• Limited to simple shapes • Lab-based
Layer removal	• Relatively simple • Stress gradient produced	• Limited to simple shapes • Destructive • Lab-based
Compliance	• Quick and simple • Portable • Low cost	• Destructive • Lab-based
Hole-drilling	• Quick and simple • Widely available • Portable • Low cost	• Destructive • Difficult interpretation • Limited resolution
Chemical probe	• Quick and simple • Portable • Low cost	• Destructive • Surface measurements
Photoelasticity	• Quick and simple • Low cost	• Must be transparent • Difficult to calibrate • No stress gradient data
X-ray	• Widely available • Non-destructive	• Composite needs to be doped with metal • Small specimens
Raman	• High resolution • Portable systems available	• Only used with carbon or Kevlar fibres • Calibration difficult
Optical fibres	• Quick and simple • Non-destructive • Portable • In situ measurements	• Embedded fibre required